# Interaction between Er atoms and the carbon cage $C_{82}$

Zhong Huang, Ling Ye, Zhong Qin Yang, and Xide Xie

*Surface Physics Laboratory, Fudan University, Shanghai 200433, People's Republic of China*
(Received 24 September 1999; revised manuscript received 22 December 1999)

The study of $Er_2@C_{82}$ by using an *ab initio* discrete-variational method based on the local-density approximation is reported. The trapping of two erbium atoms has caused significant rearrangement of the energy levels of the cage throughout the band. Due to the localized characteristic of $4f$ electrons of erbium, the on-site Coulomb interaction, "Hubbard $U$ term," is taken into consideration and the local-spin-density approximation $+U$ method is used to investigate the behavior of $4f$ electrons of Er and the electronic structure of $Er_2@C_{82}$. The description of the electronic structure of this system is greatly improved after taking on-site Coulomb interaction into consideration, and the $4f$ states are split into lower occupied states and higher unoccupied states and the splitting is 4.9 eV. Four new peaks appear below the Fermi level, and this result is in agreement with absorption spectra of $Er_2@C_{82}$. It is shown that the valence of Er ions in $Er_2@C_{82}$ is divalent and in $C_{82}$ cage the Er ion has a magnetic moment of $9.59\mu_B$. The characteristics of the states near the Fermi level are discussed.

## I. INTRODUCTION

Endohedral fullerene is a new material that provides a good prototype to study some encapsulated metal atoms. Since the first endohedral fullerene was confirmed by x-ray experiments, endohedral metallofullerenes have attracted wide attention. Alkaline, lanthanide, and transuranic metal atoms are trapped into fullerene cages, and molecules, such as $Sc_2@C_{84}$,[1] $Sc_2@C_{74}$,[2] $Dy@C_{82}$,[3] and $Gd@C_{82}$,[4] are produced and investigated widely. Many new and interesting phenomena are found in these new materials. Recently, $Er_2@C_{82}$ was made by vaporizing a mixture of carbon rods and Er oxide, and 1.5-$\mu$m infrared fluorescence of the $Er_2@C_{82}$ was observed.[5,6] Studies on the fine structure show that there exists an exchange interaction between the Er ions and the $C_{82}$ cage. Actually the $C_{82}$ cage provides an excellent setup to investigate the interaction of the Er-ion pairs.[5] Until now, as far as we know, no theoretical study on the electronic structure of $Er_2@C_{82}$ was reported. Thus it is interesting to study the geometry and electronic structure of $Er_2@C_{82}$.

To investigate endohedral fullerenes theoretically, both the cage structure and the location of the encapsulated atoms should be optimized so that the electronic properties of $Er_2@C_{82}$ can be determined. However, for lanthanide metals, there is one difficulty that the conventional local-density approximation (LDA) method cannot work well in calculating the electronic structure of $4f$ electrons. In the present work, a local-spin-density approximation (LSDA)$+U$ method, in which the on-site Coulomb interaction is taken into consideration, is used to study the electronic structure of $4f$ electrons of encapsulated Er atoms. This method has been proved by many authors[7,8] to be effective and successful in describing localized electrons of transition metals and rare earth metals. The method is incorporated into the discrete-variational (DV) cluster program of the present work.

## II. METHOD AND MODELS

The method used in this work is the DV self-consistent multicenter-multipolar method. In this DV method, a self-consistent multicenter-multipolar representation of the density is introduced. The Hamiltonian matrix elements and the overlap matrix elements (and therefore, the wave function and the charge density) are all given by numerical values on a set of sampling points. The wave functions of the cluster are expanded variationally in symmetrized atomic basis functions, which are generated self-consistently in numerical form. The detailed description of this method can be found in the literatures.[9] The von Barth–Hedin exchange-correlation potentials[10] are adopted. In the present calculations, the $4f$, $5d$, and $6s$ electrons of Er atom and the $2s$ and $2p$ electrons of the carbon atom are treated as valence electrons. The starting valence configurations of Er and C are $4f^{11}5d^16s^2$ and $2s^12p^3$, respectively.

The model for $Er_2@C_{82}$ is an isolated cluster. This system in our calculation has $C_{2v}$ symmetry. Due to the fact that the symmetry of $Er_2@C_{82}$ is not clearly known experimentally,[5] the symmetry of $C_{82}$ is taken as the symmetry of $Er_2@C_{82}$. According to a theoretical study by Nagase *et al.*[11] on $C_{82}$, there are nine $C_{82}$ isomers that satisfy the isolated pentagon rule,[12,13] and their symmetries are $C_2$, $C_3$, $C_{3v}$, and $C_{2v}$. Seven of them are used to interpret the NMR analysis by Achiba and co-workers.[14,15] The stability of these isomers is well discussed by Nagase *et al.*[11] Their calculation shows that the isomer with $C_2$ symmetry is the most stable isomer, but the stability of endohedral fullerene is different from empty fullerene. According to another theoretical calculation of Nagase *et al.* on the $M@C_{82}$ system ($M=La, Y, Sc$), the most stable monometallofullerences $M@C_{82}$ has $C_{2v}$ symmetry. Certainly $M@C_{82}$ is different from $M_2@C_{82}$. In this paper, $C_{2v}$ symmetry is adopted to investigate the geometry and electronic structure of $Er_2@C_{82}$. The two doping erbium atoms are put on the $C_2$ axis. The C-C bonds are 1.399 and 1.433 Å. The bonds of the pentagon are long bonds, while hexagons have both long bonds and short bonds according to whether the adjacent polygons are pentagons or hexagons. This structure is shown in Fig. 1. The top of this cage is a C-C bond and four adjacent hexagons, and the bottom is a
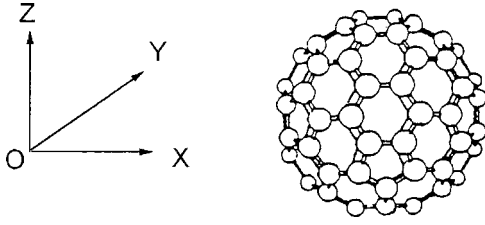
FIG. 1. Geometry of the $C_{82}$ cage with $C_{2v}$ symmetry. $C_2$ is along the $Z$ axis. The $X$-$Z$ plane is a vertical mirror plane.

hexagon. Since the bottom hexagon has two pentagons and four hexagons as its neighbors, it has four short bonds and two long bonds. The $C_2$ axis passes through the center of the top C-C bond and the bottom hexagon. The $Z$ axis is along the $C_2$ axis. The $X$-$Z$ plane is the vertical mirror plane of the cage.

In order to investigate the electronic structure of trapped Er atoms, both LDA and LSDA$+U$ methods[16] are adopted. Due to the strong localized character of $4f$ electrons, the LDA method is not good enough to describe the correlation interaction. Here the LSDA$+U$ method is incorporated in the DV cluster method. The total energy functional of LSDA$+U$ is given as[16]

$$E=E^{LSDA}+\frac{1}{2}\sum_{m,m',\sigma}U(n_{m,\sigma}-n^0)(n_{m',-\sigma}-n^0)$$
$$+\frac{1}{2}\sum_{m,m'(m\neq m'),\sigma}(U-J)(n_{m,\sigma}-n^0)(n_{m',\sigma}-n^0),$$
$$(1)$$

where $E^{LSDA}$ is the conventional LSDA total energy, $U$ and $J$ are the on-site Coulomb energy and the exchange energy, respectively, $m$ and $m'$ are the localized molecular orbitals, and $n_{m,\sigma}$ is the occupancy of the localized molecular orbital $m$ with spin $\sigma$. For simplification and as an approximation we assume that $U$ and $J$ are independent of the orbital parameter $m$. Here the average occupation of localized orbitals is approximated as $n^0$ and can be calculated by the following equation:

$$n^0=\sum_{\sigma,m}n_{m,\sigma}/k,\qquad(2)$$

where the $k$ is the total number of localized molecular obitals. Similar to the formulation of conventional LSDA, the single-particle potential can be derived from the total energy equation (1) in the following form:

$$V_{m,\sigma}=V^{LSDA}+U\sum_{m'}(n_{m',-\sigma}-n^0)$$
$$+(U-J)\sum_{m\neq m'}(n_{m',\sigma}-n^0),\qquad(3)$$

where $V^{LSDA}$ is the conventional LSDA potential corresponding to the charge density with the number of $f$ electrons given by $n_f=\Sigma_{m,\sigma}n_{m,\sigma}$. The parameter $U_f$ and $J$ of Er atoms are chosen to be 6.50 and 0.70 eV, respectively, which are obtained from $U_{eff}$ and $J$ of Anisimov, Zaanen, and Anderson.[16]
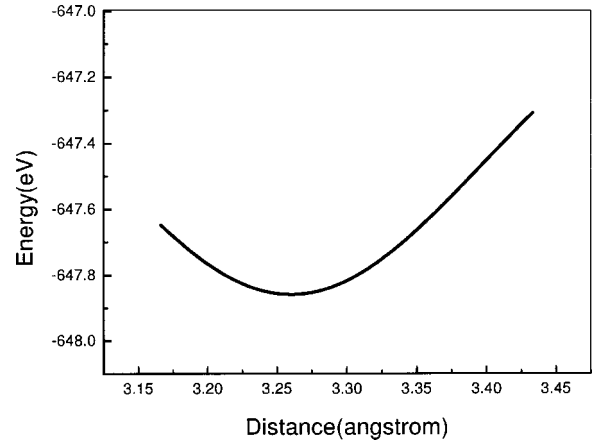


FIG. 2. Change of total binding energy vs the distance between two Er atoms.

## III. RESULTS AND DISCUSSION

### A. The geometric structure of $Er_2@C_{82}$

To optimize the positions of Er atoms in the carbon cage, the two Er atoms are placed on the $C_2$ axis and moved along the $C_2$ axis, and the most stable positions of these two Er atoms are found. The upper Er atom is 2.210 Å from the center of the top bond of the cage, and the lower Er atom is 2.240 Å from the center of the bottom hexagon plane. The distance between the two Er atoms is 3.262 Å. Figure 2 shows the change of total energy versus the distance of the two Er atoms. The C-Er bond length between the upper atom and the nearest carbon atoms are 2.407 and 2.734 Å, while the C-Er bond length between the lower atom and the nearest carbon atoms are 2.607 and 2.656 Å. According to the calculation of Nagase $et$ $al.$[17] the bonds between the encapsulated metal atoms of dimetallofullerenes and the carbons are 2.470–2.489, 2.433–2.475, and 2.567–2.589 Å for $Sc_2@C_{80}$, $Y_2@C_{80}$, and $La_2@C_{80}$, respectively, and the distances between the two caged metal atoms are 3.655, 3.922, and 3.631 Å for $Sc_2@C_{80}$, $Y_2@C_{80}$, and $La_2@C_{80}$, respectively. The results of the present work show that it is similar to the case of $Er_2@C_{82}$. The distance between the two Er atoms is shorter than the atomic diameter (3.468 Å) of Er but longer than the covalent diameter (3.120 Å) of the Er atom. Figure 3 is the charge-density contour plot on the vertical mirror plane of empty $C_{82}$, which contains five C-C bonds and the marked numbers are the charge density in units of $10^{-3}e$/a.u.$^3$ Figure 4 is the charge-density contour plot of $Er_2@C_{82}$ on the same plane and the marked numbers are also the charge density in units of $10^{-3}e$/a.u.$^3$ After trapping two Er atoms, the charge contours near the Er atoms and neighboring carbon atoms are distorted. No obvious distortion for the charge distributions is found in other carbon atoms. The charge density between the pair of Er atoms is weaker compared with that within the region of C-Er bonds. It means that there exists a relatively weaker interaction between the pair of Er atoms. This also indicates that the Er-C interaction plays a dominant role in describing the characteristics of the electronic structure of $Er_2@C_{82}$. The binding energy of one Er atom in the $C_{82}$ cage is defined as

$$E=\frac{1}{2}\{E(Er_2@C_{82})-[E(2Er)+E(C_{82})]\}.\qquad(4)$$
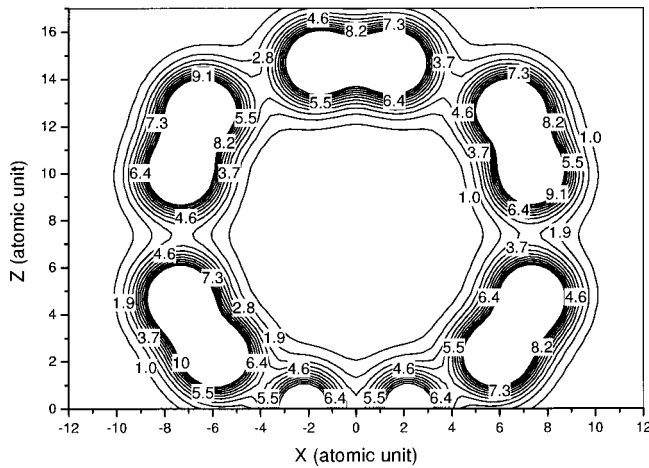
FIG. 3. Charge contour plot on the mirror plane of $C_{82}$ containing five C-C bonds. The charge density is given in $10^{-3}e/\text{a.u.}^3$

According to the LDA calculation, the binding energy per Er atom in the optimized structure of $Er_2@C_{82}$ is 9.50 eV. Comparing with the calculation of Nagase and Kobayashi[21] on the dimetallofullerene $Sc_2@C_{74}$, which shows that the binding energy of per Sc atom is 6.68 eV, the heavier rare earth metal Er has a larger binding energy than the transition-metal Sc atom, despite the fact that double Sc atoms are trapped a smaller cage $C_{74}$. The two Er atoms are also put on other axes that are perpendicular to the $C_2$ axis and parallel to the $X$ or $Y$ axis, and the optimization process is carried out. It is found that the Er atoms on the $C_2$ axis is the most stable situation.

## B. The electronic structure of $Er_2@C_{82}$

The result of the LDA calculation shows that the valence configuration of Er is $4f^{11.43}5d^{0.67}6s^{0.00}$. The Er atoms lose their two $6s$ electrons, and the $5d$ orbital can keep $0.67e$, while $0.43e$ is backtransferred to $4f$ orbitals. This configuration indicates that the valence electrons mainly show $4f$- and $5d$-like character in $Er_2@C_{82}$. The valence bandwidth is 21.00 eV, and the gap between the highest occupied molecular orbital (HOMO) and the lowest unoccupied molecular orbital (LUMO) is 0.15 eV after doping. Figures 5 and 6 are
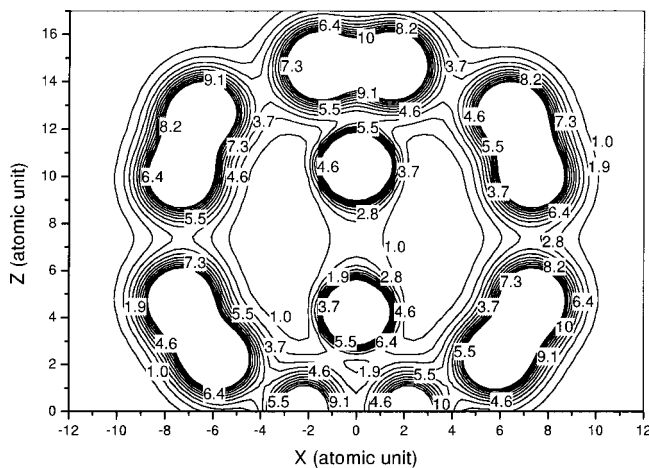


FIG. 4. Charge contour plot of $Er_2@C_{82}$ on the same plane as Fig. 3. The charge density is given in $10^{-3}e/\text{a.u.}^3$
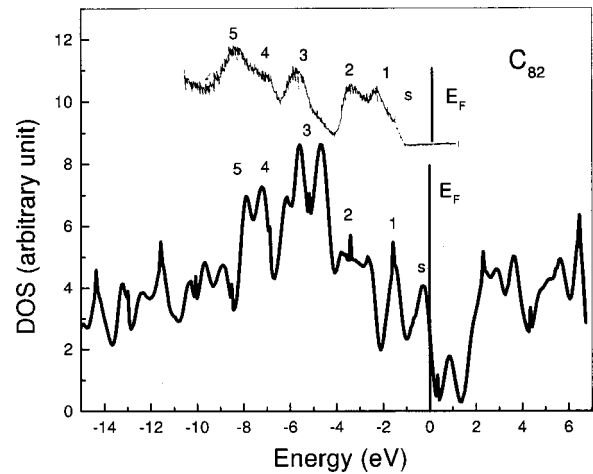


FIG. 5. Density of states of $C_{82}$. The inset is the XPS of $C_{82}$.

the density-of-states (DOS) plots of the calculation result of the LDA for $C_{82}$ and $Er_2@C_{82}$, respectively. Figure 5 gives a comparison of the calculated total DOS (TDOS) of the empty cage with the x-ray photoelectron spectroscopy (XPS) of an empty cage.[18] The inset is the XPS of $C_{82}$. By comparison, it can be seen that the five main peaks within 10 eV below the Fermi level are clearly presented and can be compared with the experimental data. In the experimental results
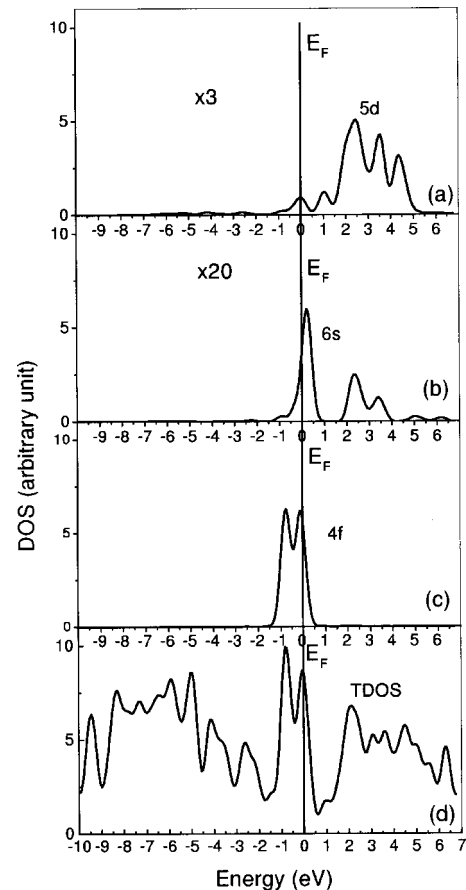


FIG. 6. Density of states of $Er_2@C_{82}$ from the LDA calculation. (a) Partial DOS (PDOS) of Er $5d$ with a scaling factor of 3; (b) PDOS of Er $6s$ with a scaling factor of 20; (c) PDOS of Er $4f$; and (d) TDOS of $Er_2@C_{82}$.
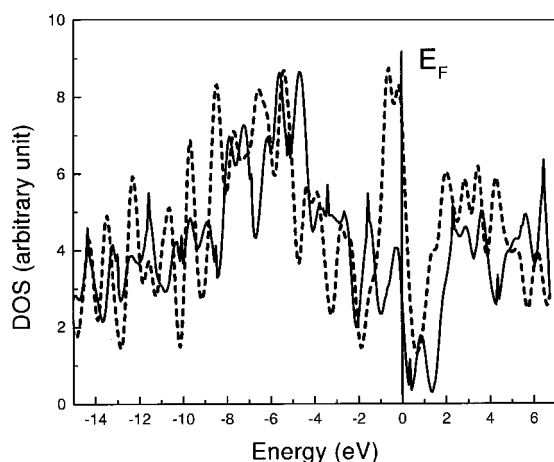
FIG. 7. Comparison of TDOS of $C_{82}$ and $Er_2@C_{82}$ in the LDA calculation. The solid line and the dashed line show the TDOS of the empty cage and that of $Er_2@C_{82}$, respectively.

there is a small shoulder labeled by ''s'' on the right-hand side of the first peak, whereas in the calculated result there is a peak also labeled as ''s'' on the right-hand side of the first peak. The gap between the HOMO and LUMO of the empty cage is very small, only 0.01 eV. Figures 6(a), 6(b), and 6(c) show the partial density of states of $5d$, $6s$, and $4f$ orbitals, respectively. Figure 7 gives a comparison of the calculated DOS of $C_{82}$ with that of $Er_2@C_{82}$. The solid line is the TDOS of the $C_{82}$ and the dashed line is the TDOS of $Er_2@C_{82}$. It shows that, after encapsulating two Er atoms and the formation of the $Er_2@C_{82}$, the TDOS of the cage changes throughout the whole band. This change is quite different from the cases of fullerenes doped with alkali-metal atoms, which shows rigid band-filling character. In the case of rigid band filling only slight changes appear in the positions of the levels after doping. Theoretical and experimental results have shown that there exists rearrangement of energy levels of the cage valence band in La@$C_{82}$.[19] In the present case, there are two atoms encapsulated in the $C_{82}$ cage, so there are more charges transferred from dopant atoms compared with La@$C_{82}$. These charges have to be rearranged in the cage valence levels. This is the reason that there exist considerable changes in the band after trapping two Er atoms in the $C_{82}$.

Figure 7 also shows that the most obvious change after trapping is that there exist double narrow and sharp peaks near the Fermi level (dashed line). It is shown in Fig. 6(c) that the main part of this double peak is from the Er $4f$ states. These localized states are located at the upper edge of the valence band and extend across the Fermi level, which means that the states near the Fermi level have a $4f$ characteristic. However, experimental results show that there exist some new cage states around the Fermi level that are caused by charge transfer from the Er atoms.[5] This discrepancy between the experimental results and calculated results is due to the fact that the system has localized $4f$ electrons, but the LDA method is not effective in treating localized electrons. So the on-site Coulomb interaction is taken into consideration to improve the description of $4f$ electrons.

The LSDA+$U$ calculation is performed on the basis of the geometry optimization by the LDA calculation. The valence configuration changes slightly after taking the on-site
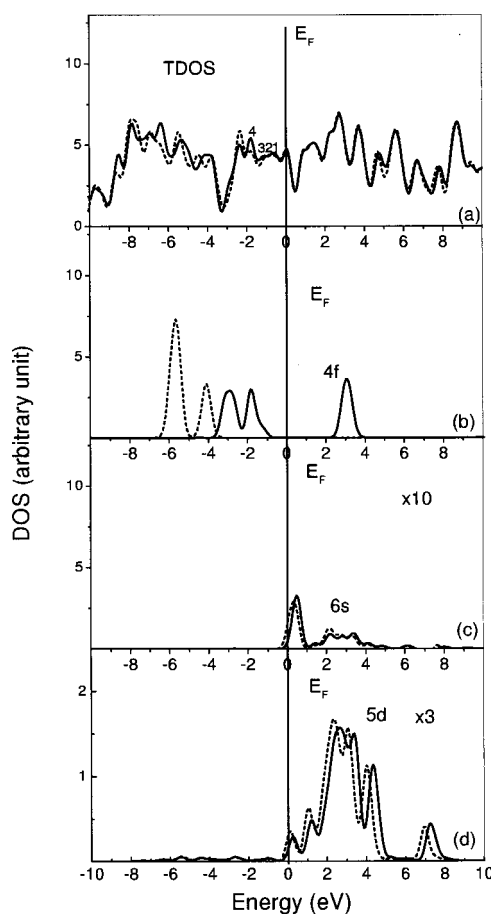


FIG. 8. Density of states of $Er_2@C_{82}$ from the LSDA+$U$ calculation. The dashed and solid lines represent the spin-up and the spin-down states, respectively. (a) TDOS of $Er_2@C_{82}$; (b) PDOS of Er $4f$; (c) PDOS of Er $6s$ with scaling factor 10; (f) PDOS of Er $5d$ with a scaling factor of 3.

Coulomb interaction into consideration. The valence configuration of Er is $4f^{11.39}5d^{0.81}6s^{0.10}$. By comparing with the LDA calculation it can be seen that $4f$ states lose a charge of $0.04e$ and $5d$ and $6s$ states gain charges of $0.14e$ and $0.09e$, respectively. As a result of the on-site Coulomb interaction, the occupied $4f$ orbitals move deeper into the lower valence band and the unoccupied $4f$ orbitals move higher up to the conduction band.

Figure 8 is the DOS calculated by using the LSDA+$U$ method. Figures 8(a), 8(b), 8(c), and 8(d) are TDOS of the $Er_2@C_{82}$, the partial density of states (PDOS) of the Er $4f$, Er $6s$, and Er $5d$, respectively. The dashed line represents spin-up states and the solid line represents spin-down states. No obvious changes have been found for the valence bandwidth 21.13 eV after using the LSDA+$U$ calculation. It can be seen from Fig. 8 that the description of states around the Fermi level has been greatly improved. Due to the rearrangement of energy levels, a 0.8-eV HOMO-LUMO gap appeared. The narrow and sharp $4f$ electronic states for the LDA calculation are split into the lower occupied states and the higher unoccupied states with a splitting of 4.90 eV. There are four peaks with the $4f$ characteristic in the occupied states, which are located at 1.84, 2.79, 4.15, and 5.71 eV, respectively, below the Fermi level as shown in Fig. 8(b). The occupied $4f$ states distribute within an energy
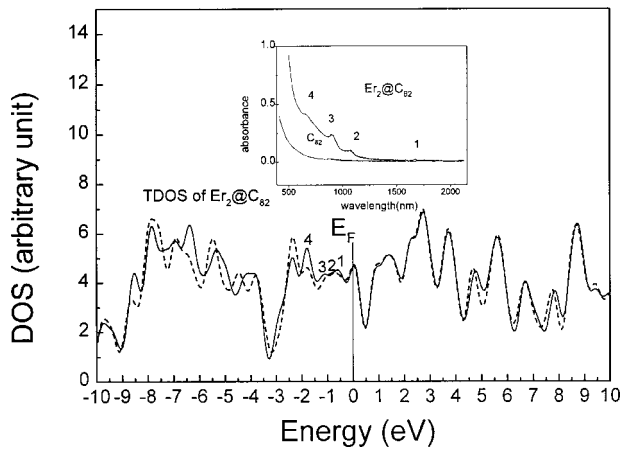
FIG. 9. Comparison between absorption spectra of $C_{82}$, $Er_2@C_{82}$, and the TDOS of $Er_2@C_{82}$ from the results of LSDA $+U$. The inset is the absorption spectra of $C_{82}$ and $Er_2@C_{82}$. The dashed and solid lines represent spin-up and spin-down states, respectively. The peaks labeled 1, 2, 3, and 4 in the TDOS of $Er_2@C_{82}$ correspond to the absorption peaks 1, 2, 3, and 4, respectively.



FIG. 10. (a) Experimental results of XPS and BIS of $4f$ states of the solid Er; (b) $4f$ PDOS of Er in the $C_{82}$ cage from the LSDA $+U$ calculation. The dashed and the solid lines represent spin-up and spin-down states in $4f$ PDOS of the LSDA$+U$ calculation, respectively.

range of 4 eV, whereas for the LDA calculation there are only very sharp double $f$ peaks. This change of $4f$ states has caused a significant effect in the total density of states of $Er_2@C_{82}$. Several new peaks appear below the Fermi level. Figure 9 is a comparison of the absorption spectra of $Er_2@C_{82}$, $C_{82}$,[5] and the calculated TDOS of $Er_2@C_{82}$ by using the LSDA$+U$ method. The upper and lower lines of the inset are the absorption spectra of $Er_2@C_{82}$ and $C_{82}$, respectively. Figure 9 shows the calculated TDOS of the $Er_2@C_{82}$, in which the dashed line represents spin-up states and solid line represents spin-down states. From the inset it can be seen that the obvious difference of absorption spectra between $Er_2@C_{82}$ and $C_{82}$ is that three peaks, at 650, 900, and 1100 nm, which correspond to energies of 1.91, 1.38, and 1.13 eV, respectively, appear after trapping two Er atoms into the cage. There is also an absorption tail from 1500 to 1700 nm in the spectra of $Er_2@C_{82}$ that corresponds to an energy about 0.80 eV.[6] In the results of the present LSDA $+U$ calculation there exist four peaks, located at $-0.65$, $-0.83$, $-1.15$, and $-1.76$ eV, labeled as 1, 2, 3 and 4, respectively, in the valence band of the TDOS of $Er_2@C_{82}$ in Fig. 8(a). The first peak in conduction band is located at 0.15 eV above the Fermi level. The electron transition from $-0.65$ to 0.15 eV corresponds exactly to the absorption tail mentioned above. Peaks 2, 3, and 4 correspond to the 1.13-, 1.38-, and 1.91-eV absorption peaks, respectively. However, in the LDA calculation, the states near the Fermi level are mainly of $4f$ character and the first conduction-band peak also shows $f$ character. The result of the LDA calculation does not agree well with the experimental results in this respect; on the other hand, the description of the electronic structure in the vicinity of Fermi level is considerably improved by the LSDA$+U$ calculation.

The unoccupied $4f$ orbitals, which in the LDA calculation distribute near the Fermi level, are now located around 3.00 eV above the Fermi level. In the LSDA$+U$ calculation, the unoccupied $4f$ states shift to higher energy levels above the $6s$ and $5d$ conduction orbitals. Although the $5d$ orbitals also
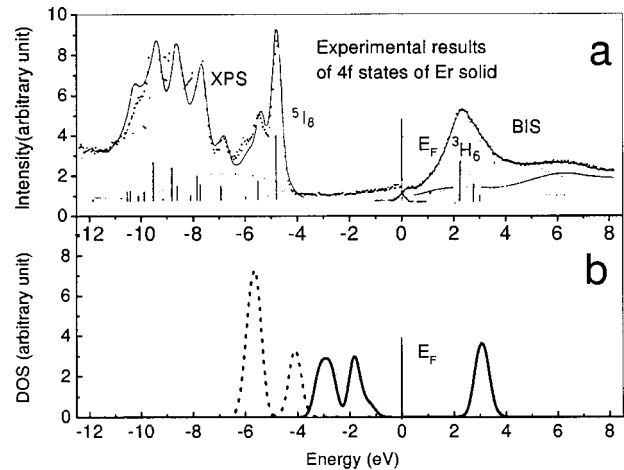
shift to high energies, there still remain some empty $5d$ orbitals in the vicinity of the Fermi level. This means that electronic hopping from occupied states to unoccupied $6s$ and $5d$ states are more favorable in energy than unoccupied $4f$ states.

In the solid states the valence of Er is trivalent; however, in the present LSDA$+U$ calculation the charge transfer of Er is $1.7e$, which means that Er in $Er_2@C_{82}$ is close to divalent. Figure 10 shows the comparison of the XPS and the bremsstrahlung isochromat spectroscopy (BIS) of $4f$ states in solid Er (Ref. 20) and the calculated $4f$ states by using the LSDA$+U$ method in $Er_2@C_{82}$. Figure 10(a) gives the XPS and BIS of the $4f$ states of solid Er, and Fig. 10(b) is the calculated DOS of $4f$ states in $Er_2@C_{82}$.[22] It can be seen that the $4f$ states of Er are located at higher energies in $Er_2@C_{82}$ than in the Er solid. Unfortunately, as far as we know, there is no experimental result for the DOS of $Er_2@C_{82}$. As a comparison, the XPS of $4f$ states of Tm doped in $C_{82}$ (inset)[23] is shown in Fig. 11. According to the $4f$ XPS Tm@$C_{82}$, the $4f$ states distribute from 1 to 6.5 eV in the
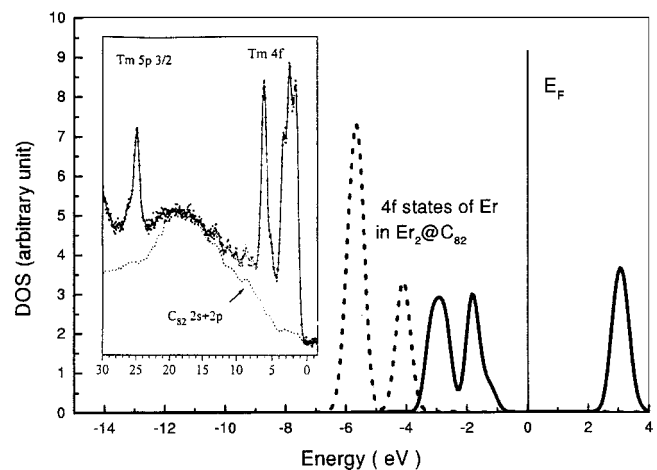


FIG. 11. LSDA$+U$ results of Er in $C_{82}$ compared to experimental XPS spectra (from Ref. 23) of Tm in $C_{82}$ (inset).

valence band. Though the $4f$ states of the Tm atom encapsulated in $C_{82}$ is different from that of Er atoms encaged in $C_{82}$, these results show that the LSDA$+U$ calculations are reasonable.

In rare earth metals, one important characteristic is that atoms have large magnetic moments. The experimental result of the value of the Er magnetic moment is $9.9\mu_B$ in the Er solid. From the present LSDA$+U$ calculation the magnetic moment of each Er atom in the carbon cage is $9.59\mu_B$, in which the contribution from $4f$ electrons, $5d$ electrons, and $6s$ electrons are $8.79\mu_B$, $0.73\mu_B$, and $0.07\mu_B$, respectively. This is reasonable, since no obvious magnetic moment exists for the fullerene cage. The Er atoms in $Er_2@C_{82}$ still have large magnetic moments, but they are less than those in the Er solid.

## IV. CONCLUSION

The electronic structures of endohedral fullerene $Er_2@C_{82}$ are studied by using an *ab initio* DV cluster method. The location of the two Er atoms in the $C_{82}$ cage is optimized. The distance between the two Er atoms is found to be 3.262 Å. The C-Er bond lengths 2.407 and 2.609 Å confirm the

fact that in the carbon cage, there exists considerable Er-C interaction in $Er_2@C_{82}$. This Er-C interaction has caused the rearrangement of the carbon-cage energy levels throughout the whole energy band. The LSDA$+U$ method is used to study the interaction between the Er $4f$ electrons and the carbon environments. The result of the LSDA$+U$ calculation shows that there exist new states in the vicinity of the Fermi level of the carbon cage after being doped by two Er atoms and that these new states correspond to the absorption peaks in the infrared and visible absorption spectra of $Er_2@C_{82}$. In the present calculation, the magnetic moment of each Er atom in $Er_2@C_{82}$ is found to be $9.59\mu_B$, which is less than but close to that of atom in Er solid. The LSDA $+U$ gives a considerable improvement on the description of the electronic structures of $Er_2@C_{82}$ compared with the LDA calculation.

[1] M. Takata, E. Nishibori, B. Umeda, M. Sakata, E. Yamamoto, and H. Shinohara, Phys. Rev. Lett. **78**, 3330 (1997).

[2] H. Shinohara, H. Yamaguchi, N. Hayashi, H. Sato, M. Ohkahchi, Y. Ando, and Y. Saito, J. Phys. Chem. **97**, 4259 (1993).

[3] G. Gu, H. Huang, S. Yang, P. Yu, J. Fu, G. K. Wong, X. Wan, J. Dong, and Y. Du, Chem. Phys. Lett. **289**, 167 (1998).

[4] S. Hino, K. Umishita, K. Iwasaki, T. Miyazaki, T. Miyamae, K. Kikuchi, and Y. Achiba, Chem. Phys. Lett. **281**, 115 (1997).

[5] R. M. Macfarlane, G. Wittman, P. H. M. van Loosdrecht, M. de Vries, and D. S. Bethune, Phys. Rev. Lett. **78**, 1397 (1997).

[6] X. Ding, J. Michael Alford, and J. C. Wright, Chem. Phys. Lett. **269**, 71 (1997).

[7] P. Wei and Z. Qing Qi, Phys. Rev. B **49**, 12 159 (1994).

[8] A. I. Lichtenstein and I. I. Mazin, Phys. Rev. Lett. **74**, 1000 (1995).

[9] Y. Ling, A. J. Freeman, and B. Delley, Phys. Rev. B **39**, 10 144 (1989); B. Delley and D. Ellis, J. Chem. Phys. **76**, 1949 (1982).

[10] U. von Barth and L. Hedin, J. Phys. C **5**, 1629 (1972).

[11] S. Nagase, K. Kobayashi, T. Kato, and Y. Achiba, Chem. Phys. Lett. **201**, 475 (1993).

[12] D. E. Manolopous and P. W. Fowler, Chem. Phys. Lett. **187**, 1 (1991).

[13] D. E. Manolopous and P. W. Fowler, J. Chem. Phys. **96**, 7603

(1992).

[14] K. Kikuchi, N. Nagahara, T. Wakabayashi, M. Honda, H. Matsumiya, T. Moriwaki, S. Suzuki, H. Shiromura, K. Saito, K. Yamauchi, I. Ikemoto, and Y. Achiba, Nature (London) **357**, 142 (1992).

[15] K. Kikuchi, N. Nagahara, T. Wakabayashi, M. Honda, H. Matsumiya, T. Moriwaki, S. Suzuki, H. Shiromura, K. Saito, K. Yamauchi, I. Ikemoto, and Y. Achiba, Chem. Phys. Lett. **187**, 1 (1991).

[16] V. I. Anisimov, J. Zaanen, and O. K. Anderson, Phys. Rev. B **44**, 943 (1991).

[17] S. Nagase, K. Kobayashi, T. Kato, and Y. Achiba, Chem. Phys. Lett. **262**, 228 (1996).

[18] S. Hino, H. Takahashi, K. Iwasaki, and K. Matsumoto, Phys. Rev. Lett. **71**, 4261 (1993).

[19] D. M. Poirier, M. Knupfer, J. H. Weaver, W. Andreoni, K. Laasonen, and M. Parrinello, Phys. Rev. B **49**, 17 403 (1994).

[20] P. A. Cox, J. K. Lang, and Y. Baer, J. Phys. F: Met. Phys. **11**, 113 (1981).

[21] S. Nagase and K. Kobayashi, Chem. Phys. Lett. **276**, 55 (1997).

[22] K. Kobayashi and S. Nagase, Chem. Phys. Lett. **282**, 325 (1998).

[23] T. Pichler, M. S. Golden, M. Knupfer, J. Fink, U. Kirbach, P. Kuran, and L. Dunsch, Phys. Rev. Lett. **79**, 3026 (1997).